Available online at www.sciencedirect.com

ScienceDirect

Physics Procedia 5 (2010) 371–380

Physics Procedia

www.elsevier.com/locate/procedia

LANE 2010

Finite Element Modelling of Laser Forming at Macro and Micro Scales

J. Griffiths*, S. P. Edwardson, G. Dearden and K. G. Watkins

Laser Group, Department of Engineering, University of Liverpool, L69 3GH, UK

Abstract

Laser forming (LF) offers the industrial promise of controlled shaping of metallic and non-metallic components for prototyping, correction of design shape or distortion and precision adjustment applications. In order to fulfill this promise in a manufacturing environment the process must have a high degree of controllability, which can be achieved through a better understanding of its underlying mechanisms. At the macro scale, Finite Element (FE) modelling can be used to ascertain which of the various process parameters associated with the temperature gradient mechanism (such as graphite burn-off, geometrical effects, variation in absorption etc) contribute towards this phenomenon and subsequently the magnitude of their contribution. At the micro scale FE modelling can be used to determine the mechanism by which deformation occurs upon application of short pulses in laser micro forming (LμF).

Keywords: Forming; TGM; FEM; pulsed lasers

1. Introduction

Laser forming (LF) is a process for the precision adjustment, shaping or correction of distortion in metallic components through the application of laser irradiation without the need for permanent dies or tools. As such it has potential for widespread application in both the manufacturing and microelectronics industry. However, for this potential to be realised, a greater understanding of the underlying mechanisms of the process is required.

The LF process involves generating thermal stresses within a substrate using a defocused beam. Depending on the desired effect, the process parameters can be altered to either induce elastic-plastic buckling or plastic compressive strains. For large scale (macro) shaping applications the most commonly employed mechanism is the Temperature Gradient Mechanism (TGM), which bends the sheet metal out of plane towards the beam. A steep thermal gradient is generated locally along the irradiation path, inducing more thermal expansion on the upper surface of the substrate. Upon cooling, providing the temperature was raised enough to cause sufficient thermal strain, plastic contraction occurs in this upper surface, creating a bend angle of 1-2^{o} per pass.

* Corresponding author. Tel.: 0151 794 4851.
E-mail address: cc0u412e@liv.ac.uk.

1875-3892
doi:10.1016/j.phpro.2010.08.064

In order to establish the required thermal gradient, the depth of heating must be relatively small compared to sheet thickness, this being achieved through an acceptable combination of traverse speed, spot size and laser power.

Initially the sheet bends away from the beam slightly as the flow stress on the upper surface is reduced. The magnitude of this counterbend is negligible compared to the resulting bend angle but is nevertheless detrimental to the process as it reduces the compressive stresses acting upon the region of plastic flow. With further heating the yield stress of the material is reached and any further expansion is converted into plastic compressive strain. Upon cooling this plastic compression is residual, and the associated conservation of volume or shortening on the upper surface causes the sheet to bend towards the beam [1].

Whilst the bend angle per pass is fairly constant initially (typically over the first 15-20 passes) there is a fall off associated with the angle of bending achieved with successive irradiations. A number of factors have been identified as contributing to this [2] and how this depends on the complex interrelation of process parameters and substrate thermo-mechanical properties.

The applicability of lasers in the micro adjustment of micro electromechanical systems (MEMS) has so far been limited due to the long thermal relaxation times associated with continuous wave (CW) and long pulse (nanosecond) lasers. Research has been conducted on non thermal LμF techniques, such as utilising shockwaves generated through the breakdown of air to induce compressive stresses in the material upper surface [3]. Providing the fluence (ϕ) is below or close to the ablation threshold (ϕ_{th}) of the material, ultra-short pulses can be used to form materials in a thermal process. When the pulse duration is shorter than the lattice interaction time, as is often the case with sub nanosecond pulses, there is little conductive heat transfer into the bulk material. This confines the heating effect to the surface layer of the material, thereby selectively inducing plastic compressive stresses and avoiding thermal damage of the substrate, as investigated in this paper.

In order for laser forming to realise its potential as a fully controlled process in a manufacturing environment an understanding of the variation in bend angle per pass is essential. At the micro scale a better understanding of the mechanism through which the application of ultra-short pulses causes plastic deformation is required. The research presented in this paper focuses on attaining a higher degree of controllability through computer based simulation and modelling as a means of process development. A full thermo-mechanical simulation of the LF process at the macro scale is presented and utilised both to identify possible process mechanisms and reduce the number of practical experiments required to characterise the process. In addition to this, a novel technique for thermal LμF involving picosecond duration pulses has been documented and its potential application in the micro adjustment of MEMS scale materials discussed.

2. Experimental

2.1. Macro scale

An experimental study of LF was conducted on graphite coated 80 x 80 x 1.5mm AISI 1010 steel coupons using a 1.5kW Electrox CO_2 TEM_{00} laser with a 3-axis Galil CNC beam delivery system, custom written control software and operating in continuous wave mode. A cantilever arrangement was used for processing, with the coupons being clamped at one edge.

To fully understand the thermal aspects of the LF process an FE model was developed. A 2005 element thermo-mechanical simulation of the laser forming of 80 x 80 x 1.5mm AISI 1010 steel, using multiple irradiations, was developed using COMSOL MultiPhysics version 3.5a (Fig 1).

Material properties were sourced from the ASM Metals Handbook, the COMSOL built in materials library and via experimentation. Thermal expansion coefficient (α_{th}), Young's modulus, Poisson's ratio, specific heat capacity (C_p), thermal conductivity (k), density (ρ) and yield stress were all considered temperature dependant and validated against empirical results. The incident laser beam was approximated by a Gaussian distributed heat source and an absorption coefficient of 0.8.

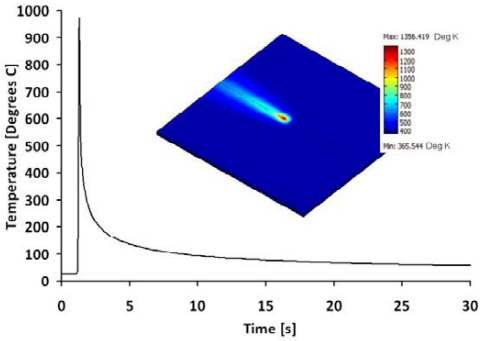

Fig. 1. Comsol MultiPhysics FE model output for the top surface directly on the laser scan line. 80 x 80 x 1.5mm mild steel AISI 1010, 760W, 5.5mm beam diameter, 35mm/s, 80% absorption, edge clamped

2.2. Micro scale

An experimental study of LμF was conducted on 1000 x 300 x 50μm AISI 302 stainless steel actuator-style arms (Fig 2) using a 3W Fianium Yb-doped fibre TEM_{00} laser with a pulse length of 20ps, operating at 1059-1069nm and 500kHz. The study comprised of adjusting the height of the actuator arms at various fluences and numbers of irradiations, using a Veeco NT1100 white light interferometer to measure the resulting bend angle. The micro-actuators were fabricated using a High-Q IC-355-800nm, 0–50kHz laser operating at 1064nm. The laser parameters used were 10kHz repetition rate, 30μJ pulse energy, 50mm/s traverse speed, 10ps pulse length and a 35μm spot diameter. The peak fluence was found to be 6.38J/cm^2. 600 irradiations were required to penetrate the material thickness.

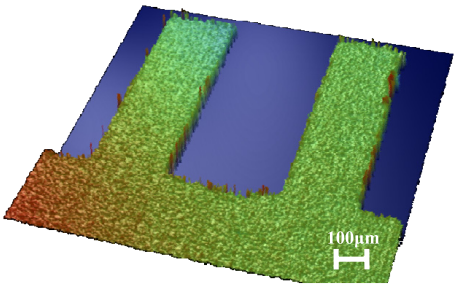

Fig. 2. 3D Veeco NT1100 white light interferometer image of 1000 x 280 x 50μm AISI 302 stainless steel actuator-style arms

3. Results

3.1. Macro scale

Numerical and experimental results and discussion on three factors which influence the bend angle per pass in macro forming are discussed in the following subsections. These factors are thermal effects, variation in absorption and geometrical effects. In addition a numerical and experimental investigation into the development of edge effects is also presented.

3.1.1. Temperature effects

With multiple irradiations an associated build up in temperature within the coupons occurs, which subsequently

affects the bend angle per pass. Such elevated temperatures can be both beneficial and detrimental and therefore a dwell time between passes must be used which best suits the process. Increased temperatures can reduce the flow stress of the component, making it easier to plastically deform. Conversely, the temperature gradient achievable between the top and bottom surface of the component along the irradiation line can be diminished, reducing the subsequent bend angle.

The magnitude of the influence that temperature effects have on the LF process is most apparent during the early stages, in this case within the first six passes. After this point thermal equilibrium between energy input and free convective cooling during the dwell time between irradiations is reached, as shown in the modelling (Fig 3). The number of passes prior to reaching this equilibrium is both material and process parameter dependant.

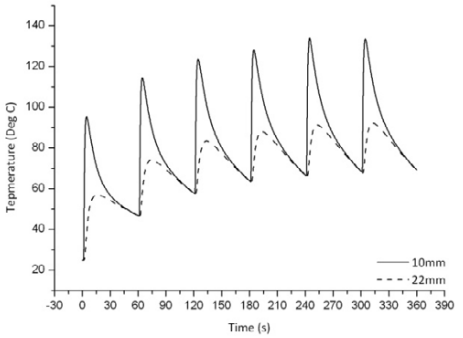

Fig. 3. FE simulation of temperature at 10mm and 22mm from the irradiation path over the first six passes. 80 x 80 x 1.5mm mild steel AISI 1010, 760W, 5.5mm beam diameter, 35mm/s, 80% absorption

The bend angle per pass for both the experiment and simulation over the first six passes reveals an initial increase prior to the fall off associated with the LF process (Fig 4).

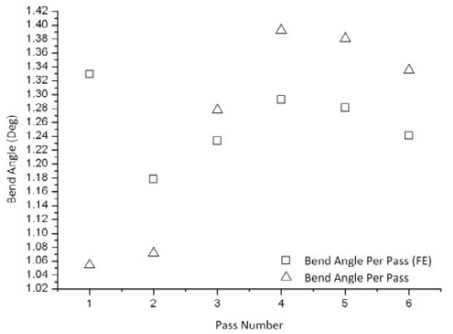

Fig. 4. Experimental and simulated bend angle per pass over the first six passes. 80 x 80 x 1.5mm mild steel AISI 1010, 760W, 5.5mm beam diameter, 35mm/s, 80% absorption

The beneficial effects of a build up in temperature appear to last up to the fourth pass before the temperature gradient is adversely affected and the bend angle per pass is reduced. An FE simulation of the first six passes was conducted in which three material thermal properties were varied within +/-20% of their initial value. These were the thermal conductivity, the specific heat capacity and the thermal expansion coefficient, with their effect on the

cumulative bend angle after six passes studied (Fig 5).

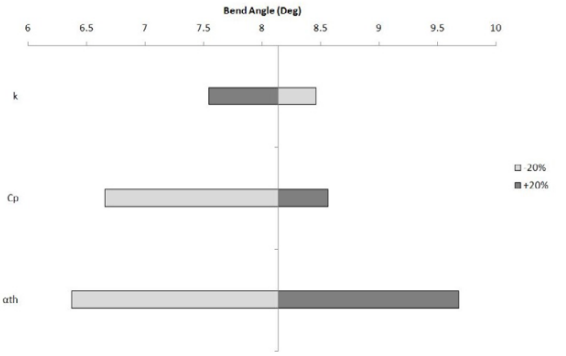

Fig. 5. Effect of varying k, C_p and α_{th} on the cumulative bend angle after six passes. 80 x 80 x 1.5mm mild steel AISI 1010, 760W, 5.5mm beam diameter, 35mm/s, 80% absorption

From Fig 5 it is clear that the thermal expansion coefficient has the largest influence on bend angle. An increase in thermal expansion subsequently increases the amount of plastic contraction that can occur upon cooling, resulting in more plastic deformation.

In assessing the effect of varying the values of k and C_p the thermal diffusivity (α) is a useful parameter to consider.

$$a = \frac{k}{\rho C_p} \tag{1}$$

The higher the value of α, the more rapidly a substrate can adjust to changes in temperature and return to a thermal equilibrium with its surroundings. Fig 6 depicts the effect on α when k and C_p are varied within +/-20% of their initial value.

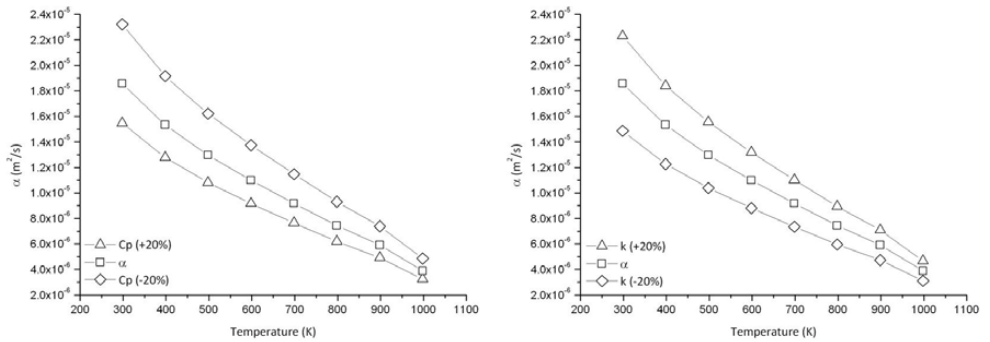

Fig. 6. The effect of varying a) C_p and b) k on α

It would appear as though in the early stages of the LF process a lower value of α is preferable.

3.1.2 Variation in absorption

Absorption effects play a key role in the LF process and as such have a large degree of influence on the bend

angle per pass. Typically, a defocused beam is employed in order to achieve sub-melting temperatures on the top surface of the component. To aid the coupling of laser radiation into the component a graphite coating is applied. Earlier research [4] has shown that with successive irradiations this coating is degraded or 'burnt off', reducing the amount of energy coupled into the component with subsequent passes. This has a direct effect on the bend angle per pass. Fig 7 shows cumulative bend angle and the bend angle per pass for both the experimental process and the analogous FE simulation.

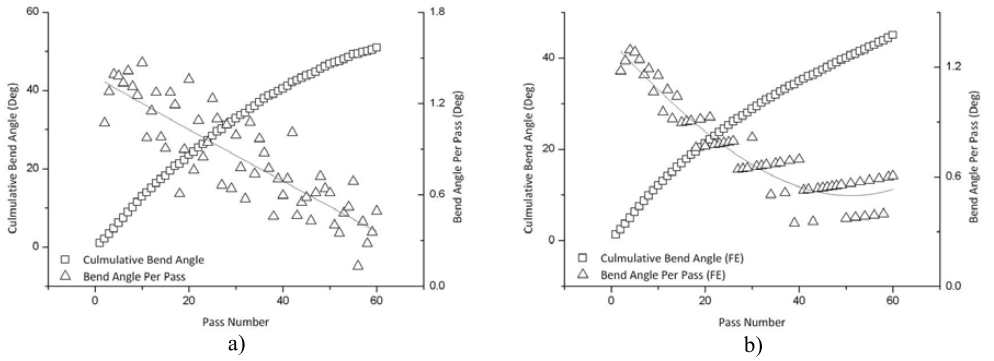

Fig. 7. Cumulative bend angle and the bend angle per pass for a) experimental and b) simulation of LF of 80 x 80 x 1.5mm mild steel AISI 1010, 760W, 5.5mm beam diameter, 35mm/s, 80% absorption

It is important to note that, in the FE simulation, the absorption coefficient is kept constant at 0.8. The simulated result is identical to the experimental result until 35 passes where it stabilises as the experimental trend continues to fall. This suggests that graphite burn off becomes detrimental to the process only after a significant number of passes. This could be due to either less energy being coupled into the component as it becomes more reflective or the loss of the secondary heat source that the burning graphite provides.

3.1.3 Geometrical effects

With increasing bend angle the initially circular beam incident on the components surface becomes more elliptical in shape [5] (Fig 8).

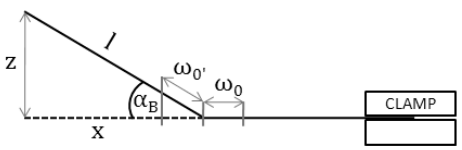

Fig. 8. The geometrical effect in LF for an edge clamped arrangement

This has the effect of reducing the energy density of the beam, with a significant reduction in power density (>20%) occurring at bend angles greater than 35°, this remaining the case regardless of spot size. The relationship between bend angle, initial beam radius and irradiation area A is described by (2).

$$A = \frac{\pi\omega_0^2 + \pi\left(\frac{\omega_0}{\cos(a_B)}\right)}{2} \tag{2}$$

A simulation was conducted in order to see the effect that such a corresponding decrease in energy density has on the initial bend angle, as depicted in Fig 9. A combination of both a Gaussian and modified Gaussian intensity distribution (3, 4) was applied to two separate boundaries along the irradiation path. The modified Gaussian distribution used separate beam radius values in the x and y axis to give the elliptical shape associated with the geometrical effect.

$$I = I_0 e^{-\left(-\frac{z\sqrt{(x.x_0)^2(y-y_0)^2}}{w_0^2}\right)} \tag{3}$$

$$I = I_0 e^{-\left[\left(-\frac{z\sqrt{(x-x_0)^2}}{w_0^2}\right)\left(\frac{z\sqrt{(y-y_0)^2}}{w_0^{2'}}\right)\right]} \tag{4}$$

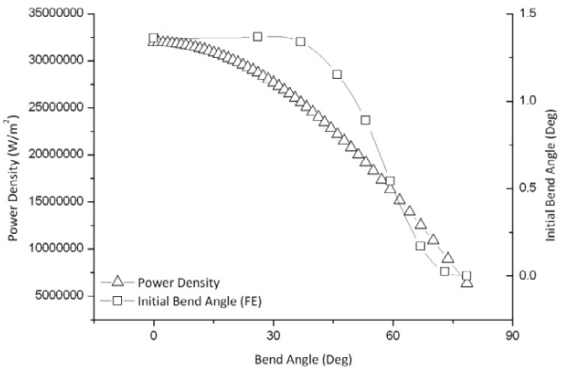

Fig. 9. Effect of reducing energy density on simulated initial bend angle. 80 x 80 x 1.5mm mild steel AISI 1010, 760W, 5.5mm beam diameter, 35mm/s, 80% absorption

From Fig 9 it can be seen that the reduction in energy density associated with the geometrical effect becomes highly detrimental at bend angles of ~35°.

3.1.4 Edge effects

A single pass FE simulation of the LF process was conducted and the development of the resultant asymmetrical edge effect [6] was monitored. This effect consists of a large inflection on the leaving edge of the plate which can be attributed to less effective conductive cooling and thus a greater amount of plastic contraction. Such asymmetrical edge effects are undesirable. A subsequent FE simulation was conducted in which the traverse speed was varied to reduce the line energy after the beam reaches the halfway point of the sheet (Fig 10). This has the effect of reducing the amount of heat which the leaving edge was required to dissipate.

Table 1. R, $D_{(max-min)}$ and α_B for both experimental and simulated single pass LF of 80x80x1.5mm mild steel AISI 1010, 760W, 5.5mm beam diameter, 35mm/s

		FE			Experimental		
V_1 (mm/s)	V_2 (mm/s)	R	$D_{(max-min)}$ (mm)	a_B (Deg)	R	$D_{(max-min)}$ (mm)	a_B (Deg)
35	35	92.524	0.011	1.205	3.921	0.131	1.162
35	37.5	104.597	0.01	1.165	26.822	0.222	1.260
35	40	116.932	0.008	1.152	95.243	0.144	1.068
35	42.5	98.271	0.067	1.08	44.221	0.0725	0.932
35	45	17857.14	0.037	1.027	274.125	0.198	0.794

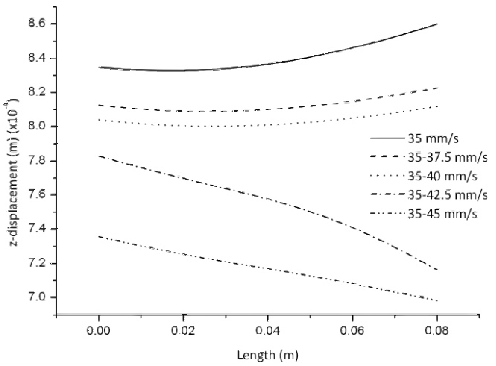

Fig. 10. Single pass FE simulation of edge effects with different scan strategies. 80 x 80 x 1.5mm mild steel AISI 1010, 760W, 5.5mm beam diameter, 35mm/s, 80% absorption

From the simulation results the optimum combination of traverse speeds was found to be 35mm/s and 40mm/s. This was confirmed by calculating the radius of curvature (R) and the difference in displacement between either edge ($D_{(max-min)}$), as in Table 1. Analogous experimentation was conducted which also found this combination of traverse speeds to be optimal.

3.2. Micro scale

Prior to thermal LμF being conducted the ablation threshold fluence (ϕ_{th}) of the stainless steel substrate was determined experimentally [7] using a 3W Fianium Yb-doped fibre TEM_{00} laser with a pulse length of 20ps, operating at 1059-1069nm and 200kHz. The average power was varied between 650-100mW and 12 holes were drilled at each power. Dwell times of 2ms and 3ms were chosen to give 400 and 600 pulses per drilled spot respectively. The diameter (D) of the ablated craters was measured using a Veeco NT1100 white light interferometer.

The beam radius was determined from a plot of D^2 against E_p and found to be 14.7μm. Using this value the fluence could be determined, and the x-intercept of a logarithmic trend line from a plot of D^2 against ϕ_0, plotted on a Log_{10} scale, was taken as ϕ_{th}. This was found to be 0.09J/cm^2 and 0.08J/cm^2 for 400 and 600 pulses respectively. Equation 5 describes the relationship between peak fluence (ϕ_0) and E_p, whilst D is related to ϕ_0 according to Equation 6.

$$\Phi_0 = \frac{2E_p}{\pi\omega_0^2} \tag{5}$$

$$D^2 = 2\omega_0 \ln\left[\frac{\Phi_0}{\Phi_{th}}\right] \tag{6}$$

Multi-pass LμF was conducted at pulse energies of 2μJ and 3μJ using a 3W Fianium Yb-doped fibre TEM_{00} laser with a pulse length of 20ps and spot diameter of approximately 20μm, operating at 1059-1069nm. The irradiation path was 100μm from the base of the arms. The use of picosecond pulse durations limited the thermal load on the bulk material whilst the high repetition rate ensured that some heat build-up occurred on the substrate upper surface.

Both a cumulative bend angle and depth of ablation were observed (Fig 11). The associated ablation can be attributed to the use of fluences above those of the experimentally determined values of ϕ_{th}.

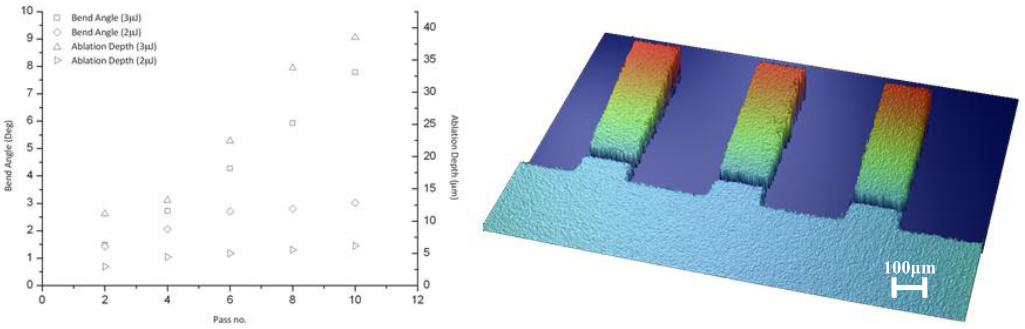

a) b)

Fig. 11. a) Cumulative bend angle per pass and ablation depth, 1000 x 280 x 50μm AISI 302 stainless steel, 500kHz repetition rate, 10mm/s traverse speed, 20μm beam diameter. b) 3D Veeco NT1100 white light interferometer image of actuator arms after 6 irradiations at 3μJ pulse energy

4. Conclusions

FE modelling of the LF process has been used to ascertain which of the various process parameters presented here (thermal effects, geometrical effects, variation in absorption) contribute towards variation in bend angle per pass with multiple irradiations and subsequently the magnitude of their contribution. Thermal effects were found to be confined to the early stages of the process, becoming less influential as thermal equilibrium is reached. Geometrical and absorption effects become dominant later in the process with increasing deformation and graphite burn-off respectively. FE simulations were used to analyse the development of undesirable asymmetric edge effects in 2D LF and subsequently devise new scan strategies to eradicate them. Analogous experimentation was conducted in order to validate these simulations.

Additionally, a thermal micro-adjustment technique employing ultra-short picosecond pulses was reported. The applicability of CW and long pulsed (nanosecond) lasers in the micro adjustment of micro electromechanical systems (MEMS) has so far been limited due to the associated long thermal relaxation times. A combination of picosecond pulse durations with high repetition rates offers a way of generating localised heat build-up on the top surface of micro-scale components. FE modeling is required in order to verify the mechanism of deformation and determine optimal process parameters.

References

1. M. Geiger and F. Vollertsen, The mechanisms of laser forming, CIRP ANNALS 42 (1993), pp. 301–304
2. S. P. Edwardson, J. Griffiths, K. R. Edwards, G. Dearden, K. G. Watkins, Laser Forming: Overview of the Controlling Factors in the Temperature Gradient Mechanism, IMechE Part C, 2010
3. Kenneth R. Edwards Stuart P. Edwardson Chris Carey Geoff Dearden Ken G. Watkins, Laser micro peen forming without a tamping layer, Int J Adv Manuf Technol (2009)
4. C. Carey, W. J. Cantwell, G. Dearden, K. R. Edwards, S. P. Edwardson, J. D. Mullett, C. J. Williams, K. G. Watkins, Effects of Laser Interaction with Graphite Coatings, Laser Assisted Net Shape Engineering 5, Lane 2007, Pp673-686
5. I. Prithwani, A. Otto, M. Schmidt, J. Griffiths, K. Watkins , S. P. Edwardson, G. Dearden, Laser Beam Forming of Aluminium Plates under Application of Moving Mesh and Adapted Heat Source, Proceedings of the Fifth International WLT-Conference on Lasers in Manufacturing 2009, Munich, June 2009
6. Jiancheng Bao, Y. Lawrence Yao, Analysis and Prediction of Edge Effects in Laser Bending, Journal of Manufacturing Science and Engineering, 54, Vol. 123, February 2001
7. P. Mannion, J Magee, E. Coyne, G. O'Conner, Ablation thresholds in ultrafast micro-machining if common metals in air, Proc. Of SPIE, Vol. 4876 (2003)